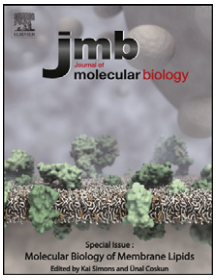

In vitro Reconstitution of a Membrane Switch Mechanism for the Polarity Protein LGL

Ilaria Visco[1,†], Carsten Hoege[2,†], Anthony A. Hyman[2] and Petra Schwille[1]

*1 - **Max Planck Institute of Biochemistry,** Am Klopferspitz 18, 82152 Martinsried, Germany*
*2 - **Max Planck Institute of Molecular Cell Biology and Genetics,** Pfotenhauerstrasse 108, 01307 Dresden, Germany*

Correspondence to Petra Schwille: *schwille@biochem.mpg.de*
http://dx.doi.org/10.1016/j.jmb.2016.10.003
Edited by Kai Simons

Abstract

Cell polarity arises from a combination of interactions between biological molecules, such as activation, inhibition, and positive or negative feedback between specific polarity units. Activation and inhibition often take place in the form of a membrane binding switch. Lethal giant larvae (LGL), a conserved regulator of cell polarity in animals, was suggested to function as such a switch. LGL localizes to both the cytoplasm and, asymmetrically, the membrane. However, the spatial regulation mechanism of LGL membrane localization has remained unclear. For systematic elucidation, we set out to reconstitute a minimal polarity unit using a model membrane, *Caenorhabditis elegans* LGL (LGL-1), and atypical protein kinase C (aPKC) supposed to activate the membrane switch. We identified a membrane binding sequence (MBS) in LGL-1 by a screen *in vivo*, reconstituted LGL-1 membrane binding *in vitro*, and successfully implemented the membrane switch by aPKC phosphorylation activity, detaching LGL from membranes. Upon membrane binding, LGL-1 MBS folds into an alpha-helix in which three regions can be identified: a positively charged patch, a switch area containing the three aPKC phosphorylation sites, and a hydrophobic area probably buried in the membrane. Phosphorylation by aPKC dramatically reduces the binding affinity of the LGL-1 MBS to negatively charged model membranes, inducing its detachment. Specific residues in the MBS are critical for LGL-1 function in *C. elegans*.

Introduction

Minimal motifs of cell polarization include one or more conventional interactions between biological molecules, such as activation, inhibition, and negative/positive feedbacks [1,2]. Many of these molecules cycle between an active membrane-bound state and an inactive cytosolic state, as in the case of cell division cycle 42 (Cdc42) in the budding yeast *Saccharomyces cerevisiae.* A single positive feedback, in which the membrane-bound molecule can self-recruit from a cytoplasmic pool, was shown to be sufficient to establish polarity *in silico* [3]. However, Cdc42 breaks symmetry and establishes polarity through a complex network of partially redundant intrinsic mechanisms in yeast cells [4]. Similarly, advective forces and mutual inhibition between the anterior and posterior partitioning-defective proteins (PAR) are known to act together with redundant symmetry-breaking inputs and positive feedback loops to robustly break symmetry in *Caenorhabditis elegans* embryos [5,6]. Lethal giant larvae 1 (LGL-1) is the main player of one of these redundant circuits and has been suggested to form a minimal polarity unit together with the anterior proteins, protein kinase C (PKC)-3 and PAR-6 [7].

In *C. elegans* embryos, LGL-1 acts redundantly with PAR-2 to maintain polarity and can compensate for PAR-2 depletion [7,8]. In contrast to PAR-2, which is only found in the genus *Caenorhabditis* [9], LGL is highly conserved in eukaryotes [10] where it takes over the role of PAR-2 in counteracting the action of the anterior PAR proteins.

The domain structure of LGL proteins is well conserved in many metazoans; the N-terminal part of the protein contains multiple WD40 domains, which fold into β-propeller structures, providing a docking platform for interaction with multiple proteins [10]. In *Drosophila*, for example, the N-terminal WD40 domain-containing part of LGL was predicted to fold into two

β-propeller structures [11] and has been shown to interact with both the C terminus of LGL itself and PAR-6 [11,12]. The C-terminal part of LGL consists of an LGL-specific domain, which contains several conserved sites for serine and/or threonine phosphorylation by atypical PKC (aPKC) [10]. It was proposed that the non-phosphorylated LGL is the active form of the protein assuming an open conformation, whereas the phosphorylated LGL is inactive because its C terminus interacts intramolecularly with the N terminus, closing the protein in an autoinhibitory state [11]. However, *C. elegans* LGL-1 does not seem to have the conserved WD40 domains, and therefore, it is unclear if a similar mechanism could act in *C. elegans*.

Interestingly, LGL-1 and PAR-2 share several common features in *C. elegans* early embryos: they both localize to the posterior cortex, their activity is regulated by PKC-3 phosphorylation, and they can exclude anterior PARs from the posterior cortex [5,6]. PAR-2 acts indirectly, recruiting PAR-1 to the membrane [13,14], which phosphorylates PAR-3 on a conserved site in the C-terminal domain [15–17]. LGL-1 is thought to act directly on PAR-6. In *C. elegans*, LGL-1 has been shown to bind PKC-3 and PAR-6 in immunoprecipitation assays [7] and regulate PAR-6 cortical accumulation and overall levels [18]. Based on this direct interaction, it is conceivable that LGL-1, PKC-3, and PAR-6 form a minimal polarity unit [7], in which the PAR-6/PKC-3/LGL-1 complex is formed at the membrane boundary between the anterior and posterior domains, where PKC-3 can phosphorylate LGL-1, causing the whole complex to leave the cortex.

We sought to shed light on the molecular mechanism of how exactly LGL-1 localizes at the membrane. We identified a region of the protein that can directly bind negatively charged membranes. The binding specificity depends on a stretch of positively charged amino acids surrounding the PKC-3 phosphorylation sites. LGL-1 membrane binding sequence (MBS) folds into an alpha helical conformation upon membrane binding. In the membrane-bound helix, three regions can be identified: a positively charged area responsible for the lipid specificity, a switch area containing the three PKC-3 phosphorylation sites, and a hydrophobic area, which is probably buried in the membrane. Phosphorylation dramatically reduces the binding affinity of the LGL-1 MBS to negatively charged model membranes, inducing its detachment. We were able to encapsulate LGL-1 MBS in giant unilamellar vesicles (GUVs) and directly visualize its phosphorylation-induced detachment from the membrane. In addition, we demonstrate that mutations in LGL-1 that remove the positive residues required for membrane binding show defects in localization and LGL-1 function *in vivo* in yeast and in *C. elegans* embryos. Thus, both LGL-1 membrane binding and binding to PAR-6/PKC-3 seem to be required to regulate the PAR domain boundary in *C. elegans* embryos.

Results

LGL-1 directly binds membranes containing negatively charged lipids via a stretch of basic amino acids

Several PAR proteins can associate with membranes [19,20]. *C. elegans* PAR-2 can directly interact with phospholipids and, in particular, with phosphoinositides *in vitro* [14]. *In vivo* localization of PAR-2 to the posterior cortex depends on a central domain rich in basic amino acids, suggesting that PAR-2 interacts with phospholipids at the plasma membrane [5,21]. In mammalian cells, LGL binding to the cell cortex is regulated by hypoxia [22], and Drosophila LGL binds the cell cortex through hydrophobic patches [23]. We wanted to investigate whether *C. elegans* LGL-1 binds to the cell cortex by associating with the plasma membrane. We performed an *in vivo* fragment screen to identify the regions of LGL-1 that can directly interact with the plasma membrane of *S. cerevisiae* (see Materials and Methods). We identified several fragments that could promote yeast growth at restrictive temperatures (Supplementary Material Fig. S1). Secondary screening showed that regions 5/6 are required for membrane binding (Supplementary Material Fig. S1). Importantly, this region contains the three phosphorylation sites for PKC-3 (S661/S665/T669), which is rich in positively charged amino acids.

We expressed the LGL-1 5/6 fragment (aa 469–702) in *Escherichia coli* as a fusion protein with enhanced green fluorescent protein (GFP; eGFP) and a hexahistidine tag (His6) and incubated it with GUVs containing different lipid mixtures. LGL-1 did not bind to GUVs containing pure 1,2-dioleoyl-sn-glycero-3-phosphocholine (DOPC), but it bound to GUVs doped with different negatively charged phospholipids (Fig. 1a–f). Among the several acidic phospholipids screened, 1,2-di-(9Z-octadecenoyl)-sn-glycero-3-phospho-L-serine (DOPS) and phosphatidylinositol 4,5-bisphosphate (PI(4,5)P2) were included since they are, respectively, the most abundant phospholipid and phosphoinositide of the cytosolic side of the cell membrane. The relative amount of each negatively charged lipid was chosen in order to maximize the overall GUVs' charge and keep it constant [24]. As a positive control, we used GUVs doped with DGS-NTA(Ni) (Fig. 1b), which is able to bind His6-tagged proteins [25]. LGL-1 5/6 was found to bind to GUVs containing DOPS or PI(4,5)P2, and phosphatidylglycerol or cardiolipin, which are usually not present in plasma membranes.

LGL-1 preferentially binds PIP2-containing membranes

Besides the numerous well-characterized globular domains that bind, more or less specifically, acidic

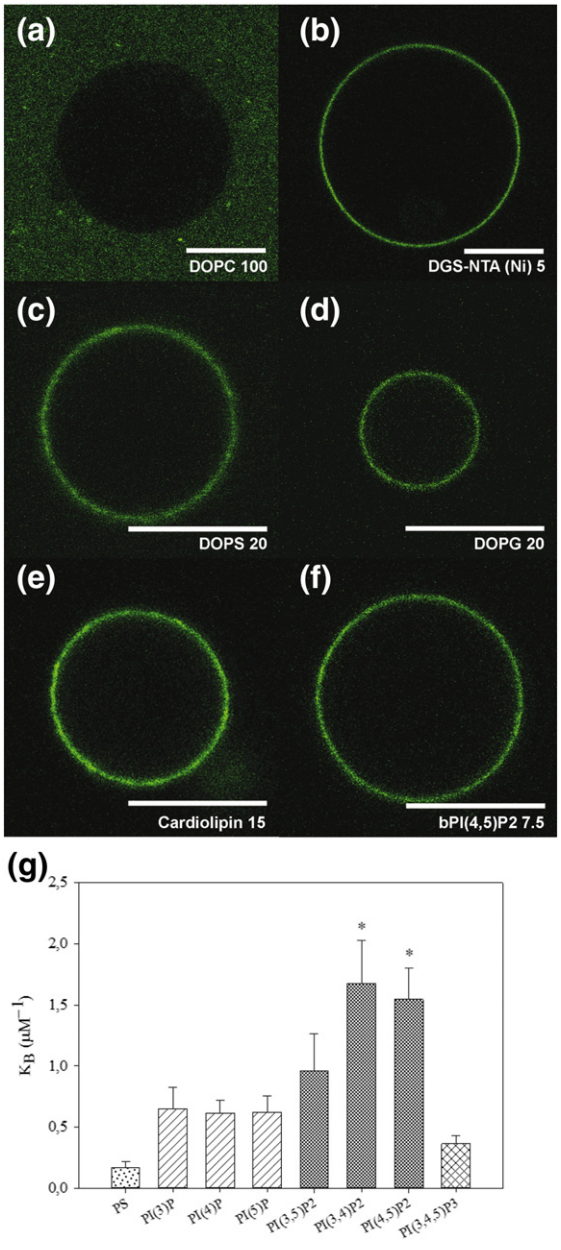

Fig. 1. LGL-1 preferentially binds PIP2-containing membranes. (a–f) Membrane binding with GUVs. LGL-1 5/6 fragment (aa 469–702):eGFP-His6 was expressed in *E. coli*, purified, and incubated with GUVs containing different lipid mixtures: (a) DOPC 100; (b) DOPC: DGS-NTA(Ni) 95:5; (c) DOPC:DOPS 80:20; (d) DOPC: DOPG 80:20; (e) DOPC:cardiolipin 85:15; (f) DOPC: bPI(4,5)P2 92.5:7.5. Scale bars represent 10 μm. (g) LGL-1 MBS was incubated with DOPC LUVs containing different acidic lipids: DOPS 5%, PI(3)P, PI(4)P or PI(5)P 2.5%, PI(3,4)P2, PI(3,5)P2 or PI(4,5)P2 1.67%, and PI(3,4,5) P3 1.25%. The relative amount of each negatively charged lipid was chosen in order to keep the overall LUVs' charge constant at 5%. (g) Mean K_B values obtained for each lipid mixture are displayed. LUVs containing either PI(3,4)P2 and PI(4,5)P2 show the highest K_B values [$^*p < 0.05$ for all comparisons except with PI(3,5)P2].

phospholipids at the membrane surface [26], short basic amino acid sequences are also known to interact electrostatically with phosphoinosites. As an example, the unstructured basic effector domain of the myristoylated alanine-rich C kinase substrate binds PI(4,5)P2 with high affinity but little headgroup specificity to form an electroneutral complex [27,28]. In order to determine whether the LGL-1 MBS binds phosphoinositides and, in particular, PI(4,5)P2 with higher affinity than other acidic phospholipids, we incubated a peptide corresponding to the LGL-1 MBS with DOPC large unilamellar vesicles (LUVs) containing DOPS or phosphoinositides and measured their electrokinetic or zeta-potential at different peptide concentrations. LUVs were used instead of GUVs because reliable zeta-potential measurements are possible only if the population of lipid vesicles is monodisperse. It was recently demonstrated that zeta-potential can be used to determine the binding affinities of positively charged peptides to negatively charged liposomes [29]. The rationale behind this approach is simple: the more peptide binds to the vesicles, the higher the zeta-potential of the vesicle–peptide complex becomes until it eventually reaches zero or positive values. Therefore, a fixed concentration of LUVs was titrated with increasing concentrations of the LGL-1 MBS peptide until saturation was reached. The zeta-potential of the vesicle–peptide complex was recorded at each concentration and plotted to make a binding curve (Supplementary Material Fig. S2B).

In contrast to the antimicrobial peptides studied by Freire and colleagues [29], the zeta-potential does not increase linearly with increasing LGL-1 MBS peptide concentrations (Supplementary Material Fig. S2B); thus, their mathematical model could not be employed to fit our data and obtain a partition coefficient. An alternative approach, which is based on the Langmuir isotherm model [30,31] and allows to extrapolate an apparent binding constant K_B from the fit of the zeta-potential curves [32], was used instead (Supplementary Material Fig. S2B). This approach assumes that the free peptide is in excess over the bound peptide and that the variation of the zeta-potential is proportional to the peptide surface coverage. The LGL-1 MBS peptide shows the highest K_B for PI(3,4)P2- and PI(4,5)P2-containing LUVs (Fig. 1g).

The position of the basic amino acids modulates LGL-1 membrane binding specificity

We further investigated the role of the positively charged amino acids of the LGL-1 MBS, observing the effect of selected mutations on membrane binding. When we systematically mutated the basic amino acids of the LGL-1 469–702 fragment to non-charged residues and tested the mutants for membrane binding in yeast, we found that R671/R672 are critical for growth at the restrictive temperature. In addition, mutations of R658/K660 showed slightly weaker growth at the

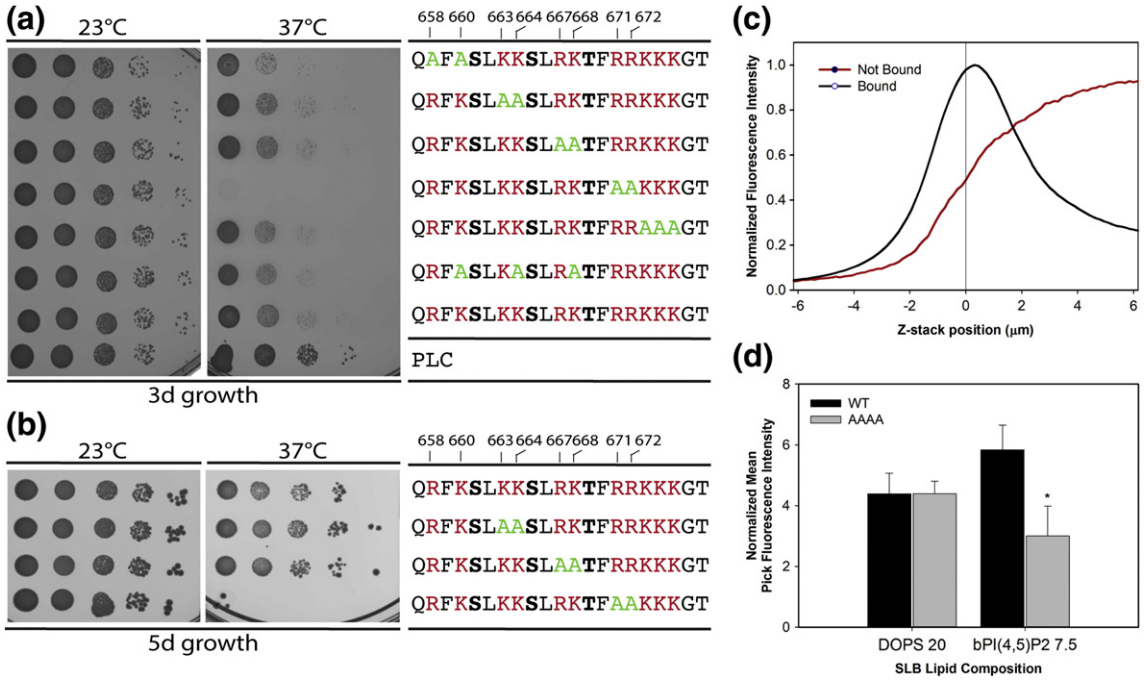

Fig. 2. LGL-1 arginines 671 and 672 are required for membrane binding. (a and b) Yeast membrane binding growth assay (a) LGL-1 5/6 fragment (aa 469–702) arginine mutant 671A, 672A does not confer growth at 37 °C, see fourth row. (b) Full-length LGL-1 requires arginines 671 and 672 for growth at 37 °C. (c and d) LGL-1(469–702):eGFP-His6 R658A/K660A/RR671AA (LGL-1-AAAA) was incubated with SLB containing different lipid mixtures: DOPC 100, DOPC:DOPS 80:20, and DOPC:bPI(4,5)P2 92.5:7.5. (c) Typical z-scans intensity profiles acquired with confocal laser scanning microscope for LGL-1 bound (black) or not bound (red) to the SLB. (d) LGL-1 fluorescence intensity values at the membrane were extracted from the peaks in z-stack intensity profiles, background corrected, averaged, and normalized by the value obtained in SLB containing DOPC only. WT = 5.83 ± 0.81, $n = 3$; AAAA = 3.00 ± 0.98, $n = 3$; *t-test $t(4) = 3.84$, $p < 0.05$.

restrictive temperature (Fig. 2a). We then made an LGL-1 5/6:eGFP-His6 fragment carrying a combined quadruple mutation R658A/K660A/R671A/R672A of the membrane binding residues (LGL-1-AAAA) and incubated it with supported lipid bilayers (SLBs) containing pure DOPC or DOPC doped with either DOPS or PI(4,5)P2. Upon binding, the fluorescence signal at the level of the SLB membrane is maximized, while the fluorescence signal in the buffer above the membrane decreases (Fig. 2c). Similar to what we observed in LUVs, LGL-1 5/6 wild type (WT) binds SLBs containing PI(4,5)P2 more than those containing DOPS (Fig. 2d, WT). Interestingly, the LGL-1-AAAA mutant maintains the ability to bind DOPS-containing membranes, whereas its binding to bPI(4,5)P2-containing membranes decreases (Fig. 2d). This suggests that the positively charged amino acids in the LGL-1 MBS are contributing to the membrane binding not only with their charges but also with their individual positions, which may account for the preferential binding to specific phosphoinositides.

LGL-1 MBS folds into an alpha-helix upon binding to negatively charged membranes

We next investigated the conformation of the LGL-1 MBS at the membrane. To do so, we measured the CD of the corresponding peptide in the absence and presence of small unilamellar vesicles (SUVs) containing different acidic lipids. Although it was reported that accurate CD spectra can be collected in the presence of LUVs [33], in our hands, the light scattering was too high to allow reliable measurements. In CD buffer or in the presence of pure DOPC vesicles, to which the peptide does not bind, LGL-1 MBS shows clear random coil CD spectra with a residual alpha-helicity of about 7% (Fig. 3a, red line). In order to check if the peptide has a propensity to fold into an alpha-helix, we acquired the CD spectra of the peptide in trifluoroethanol (TFE), which is known to stabilize secondary structure, strengthening the peptide H-bonds [34]. In TFE, LGL-1 MBS shows a clear alpha-helix CD spectrum with the two characteristic minima at 208 and 220 nm (Fig. 3a, blue line). The alpha-helix content was estimated to be ca 66%. Similar CD spectra were obtained when the LGL-1 MBS peptide was mixed with SUVs containing acidic lipids (Fig. 3a, green/gray/yellow lines). The estimated alpha-helix content increases with increasing vesicle: protein ratios (Fig. 3b and Supplementary Material Figure S4), strongly suggesting that the peptide folds into an alpha-helix upon binding to negatively charged vesicles. The isodichroic point in this type of CD spectra indicates that there are only two peptide

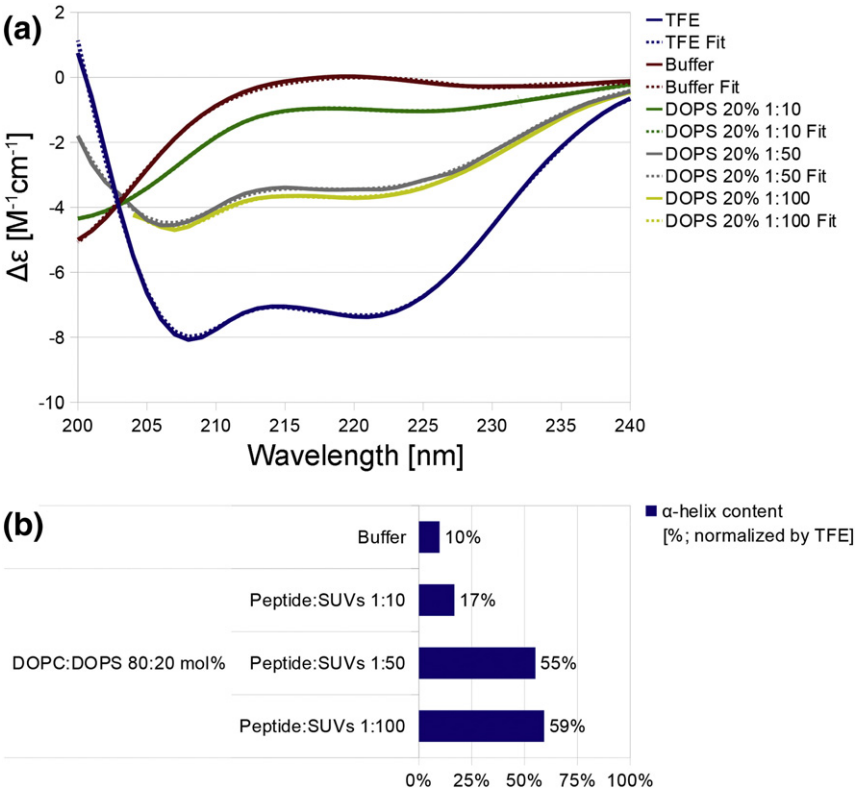

Fig. 3. LGL-1 MBS folds into an alpha-helix upon binding to negatively charged membranes. (a) CD spectra (data, continuous lines; fits, dashed lines) of LGL-1 MBS in CD buffer, TFE, and in the presence of different protein:lipid ratios of DOPC:DOPS 80:20 SUV. (b) Alpha-helix content estimated with the CONTIN method was normalized by the value obtained in TFE and was plotted for each spectrum in (a).

populations: disordered in solution and largely helical at the membrane [35]. LGL-1 MBS conformation is different from what was described for the basic effector domain of myristoylated alanine-rich C kinase substrate, which binds the membrane in an extended conformation with the five phenylalanine residues penetrating to the level of the acyl side chains [36].

Phosphomimetic LGL-1 does not bind GUVs containing negatively charged lipids

Having demonstrated that LGL-1 can directly bind lipid membranes, we hypothesized that the phosphorylation by PKC-3 directly interferes with its membrane binding ability. This hypothesis was supported by *in vivo* membrane binding results of the LGL-1 AAA and EEE mutant in yeast, in which the phosphomimetic EEE mutant does not support membrane binding (Fig. 4e).

We repeated the GUV binding assay with purified LGL-1 proteins, which carried either the AAA or the EEE mutation. Similar to what was described for the LGL-1 WT, we incubated the LGL-1 mutants with GUVs containing PI(4,5)P2. As expected, LGL-1 AAA retains its ability to bind GUVs, whereas EEE does not. (Fig. 4a–d).

Phosphorylation of LGL-1 inside GUVs induces its detachment from the vesicle membrane

In order to confirm that LGL-1 can be phosphorylated *in vitro* by PKC-ζ [37] and to optimize the phosphorylation conditions, we phosphorylated the LGL-1 MBS peptide *in vitro* and visualized the experiment by autoradiography (Supplementary Material Fig. S5). Importantly, in the LGL-1 AAA mutant, in which serines/threonines were mutated, phosphorylation was absent.

Both phosphorylated and non-phosphorylated LGL-1 MBS peptides were encapsulated in GUVs using the droplet transfer method [38–40]. For these experiments, we used DOPS instead of PI(4,5)P2, because the phosphoinositide has a poor solubility in oil due to its strong negative charge [41]. Although the affinity of the LGL-1 MBS peptide for DOPS is 1 order of magnitude lower than for PI(4,5)P2 (Fig. 1g), we do not expect a different behavior upon phosphorylation. The components for the kinase reaction used to phosphorylate LGL-1 MBS in the radio assay were encapsulated in DOPS-containing GUVs either in the

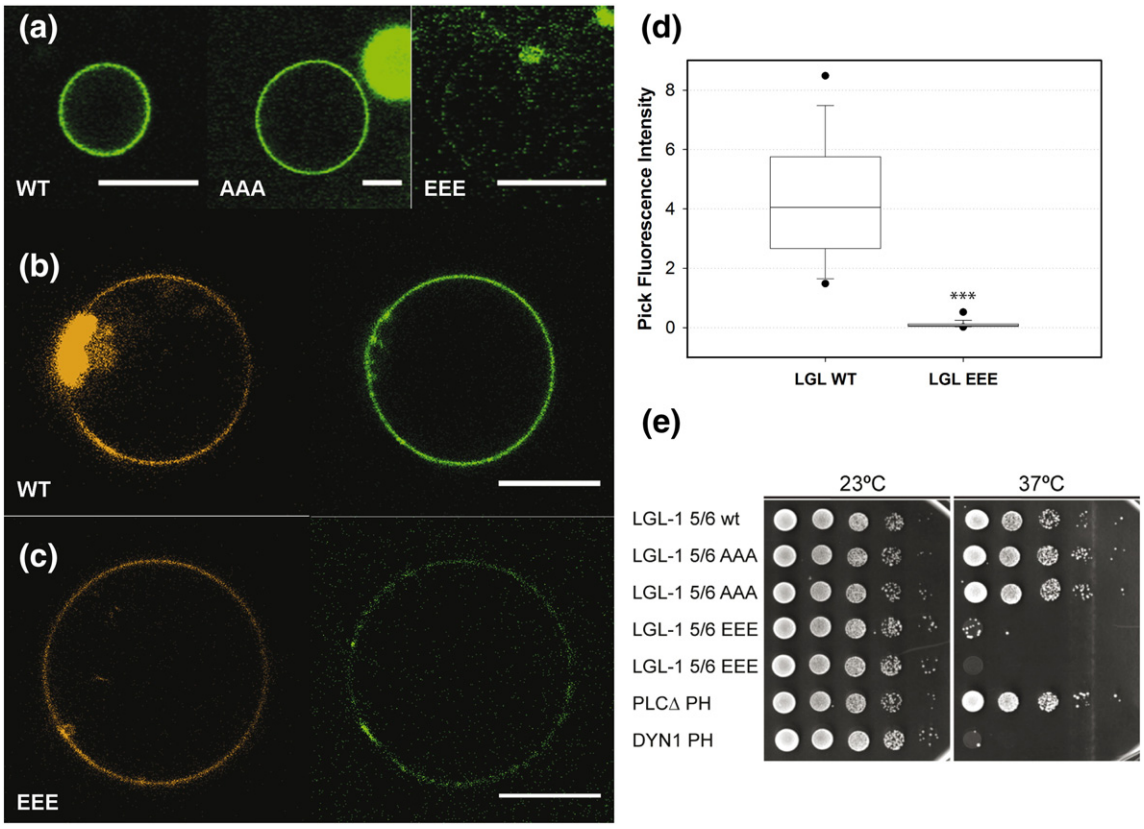

Fig. 4. LGL-1 phosphomimetic mutant S661E, S665E, T669E does not bind acidic membranes. (a–d) Membrane binding with GUVs. LGL-1(469–702):eGFP-His6 WT and its phosphorylation mutant S661A, S665A, T669A (AAA) and phosphomimetic mutant S661E, S665E, T669E (EEE) were expressed in *E. coli*, purified, and incubated with GUV containing DOPC:bPI(4,5)P2 92.5:7.5 as a lipid mixture. (b and c)Texas Red DHPE was used as a lipid dye. GUVs were imaged at the equator with a confocal laser scanning microscope. Scale bars represent 10 μm. (d) Intensity radial profile plots were determined for each GUV, and peak values were plotted. WT = 4.37 ± 2.24, $n = 62$; EEE = 0.15 ± 0.33, $n = 61$; ***t-test, $t(121) = 14.549$, $p < 0.001$. (e) The phosphorylation mutant AAA confers growth in a yeast membrane binding assay, whereas the phosphomimetic mutant EEE does not. PH domain of PLC is a positive control and DYN1 PH is a negative control.

presence or in absence of ATP. As expected, the peptide binds the membrane in the mixture without ATP (Fig. 5a). In contrast, LGL-1 MBS appears homogeneously distributed inside the GUVs and does not bind the inner membrane when ATP was present in the kinase mixture, that is, when human PKC-ζ could phosphorylate the LGL-1 MBS peptide (Fig. 5b).

For triggering phosphorylation *in situ* inside the GUVs, the reagents need to enter the lumen of the GUV from the outside medium. To achieve that, alpha-hemolysin was used to form pores in the GUVs [39] (See Materials and Methods). Once pores are formed, ATP and $MgCl_2$ are sequentially added to the external solution to trigger the phosphorylation of the LGL-1 MBS peptide. LGL-1 originally localizes at the membrane inside the GUV where it remains after the addition of both alpha-hemolysin and ATP (Fig. 5c–e). However, it detaches after the addition of $MgCl_2$, when the kinase reaction is triggered (Fig. 5f).

The same experiment was repeated with GUVs containing 20%mol DOPS. At high charge density, the distribution of the LGL-1 MBS peptide between free and bound state is strongly shifted to the bound state (Supplementary Material Fig. S6). In this condition, PKC-ζ does not phosphorylate enough substrate to influence the overall peptide distribution in the time scale of the observation. Therefore, the unbinding of LGL-1 does not take place, suggesting that the peptide is not accessible for the human PKC-ζ. A similar observation was made for PAR-2 binding to lipid strips, whose interaction with microtubules is sufficient to protect it from the action of aPKC [14]. This mechanism of protection could also explain why in some GUVs, LGL-1 MBS only partially remains at the membrane, forming a domain that shrinks with time until it eventually disappears (Supplementary Material Fig. S7).

Taken together, these findings support the hypothesis that the phosphorylation by aPKC or the

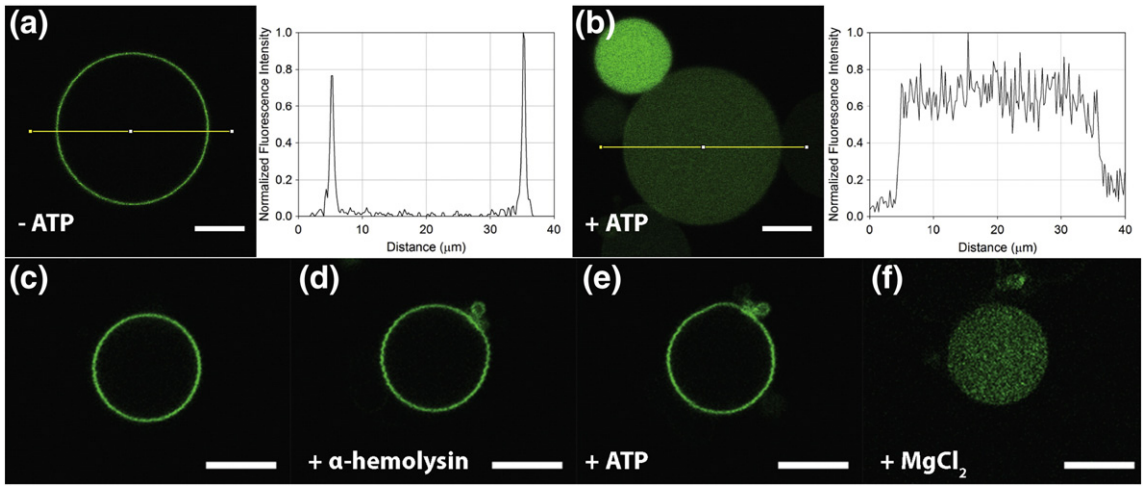

Fig. 5. Reconstitution of LGL-1 phosphorylation in GUVs. The same kinase reaction used to phosphorylate LGL-1 MBS in the radio assay was encapsulated in GUV containing 20%mol DOPS either in the (a) absence or (b) presence of ATP. (c–f) Images of representative GUVs are reported with their corresponding normalized intensity profiles. (c) *In situ* LGL-1 phosphorylation inside a GUV LGL-1 MBS was encapsulated in GUV containing 5%mol DOPS. (d) Alpha-hemolysin, (e) ATP, and (f) $MgCl_2$ were sequentially added to the external solution. Scale bars represent 10 μm.

phosphomimetic mutations of the PKC-3 sites interferes with the binding of LGL-1 to negatively charged lipids.

LGL-1 membrane binding mutants have compromised function *in vivo*

When we aligned the LGL-1 MBS protein sequences from different metazoans, we found that the basic residues that are required for membrane binding are highly conserved (Supplementary Material Fig. S8). When we expressed full-length LGL-1 in our yeast *in vivo* membrane assay, it supported growth at restrictive temperatures, indicating membrane binding. However, when we mutated residues R671 and R672 to alanines, growth was not supported, indicating that membrane binding was lost (Fig. 2b).

We wanted to confirm our results by expressing LGL-1 fused to GFP in yeast cells. LGL-1-GFP is strongly enriched at the plasma membrane, but LGL-1-GFP membrane localization is lost when R671 and R672 were mutated to alanines. This indicated that these two residues are sufficient to localize the protein to the plasma membrane *in vivo* (Fig. 6a).

In *C. elegans* embryos, it is assumed that membrane localization is required for LGL-1 function. A phosphomimetic LGL-1 variant (EEE) does not localize to the membrane and is not functional in maintaining two PAR domains. However, a mutant in which the serine and threonine residues are mutated to alanines (AAA phos. mutant) localizes to both the anterior and posterior membrane but is not able to maintain PAR domains either. Therefore, it seems likely that LGL-1 needs to undergo phosphorylation cycles to maintain PAR domains, and we suggested that LGL-1 functions at the PAR domain boundary by mutual elimination [7].

To see how LGL-1 membrane binding mutants affect LGL-1 function, we mutated R671 and R672 to alanines and looked at GFP-LGL-1 R671A, 672A transgenic localization in the early embryo. Surprisingly, and in comparison to yeast, the mutant LGL-1 localized similarly as WT LGL-1 to the membrane, indicating that LGL-1 has additional membrane binding sites (region 5; Supplementary Material, Fig. S1), is recruited by endogenous LGL-1, or binds to an unknown membrane or cortex protein for membrane localization. However, when we depleted PAR-2 in embryos expressing GFP-LGL-1, we saw that, in comparison to GFP-LGL-1 wt, GFP-LGL-1 R671A, 672A could not maintain localization at the membrane and that cell polarity was lost (Fig. 6b).

When we compared embryo lethality of GFP-LGL-1 WT or GFP-LGL-1 R671A, 672A expressing embryos, in which we depleted PAR-2, we found that embryo lethality is very small in embryos expressing GFP-LGL-1, because LGL-1 can compensate for PAR-2 function [7,8]. However, lethality is very high in embryos expressing the GFP-LGL-1 R671A, 672A mutant (Fig. 6d). This indicates that indeed membrane binding by R671 and R672 is required to maintain PAR domains in the early *C. elegans* embryo.

LGL-1 binds to the membrane, and its phosphorylation is required for its function in polarity. LGL-1 also interacts with both PAR-6 and PKC-3, and we wanted to study whether the LGL-1 membrane binding mutations affect this interaction. We performed immunoprecipitations with GFP-LGL-1 WT or GFP-LGL-1 R671A, 672A (AA) and GFP-LGL-1 R658A, K660A, R671A, R672 (AAAA) from protein extracts of early *C. elegans* embryos. Whereas GFP-LGL-1 WT interacts with both PAR-6 and PKC-3 as seen previously [7], we found that the membrane binding mutants AA and

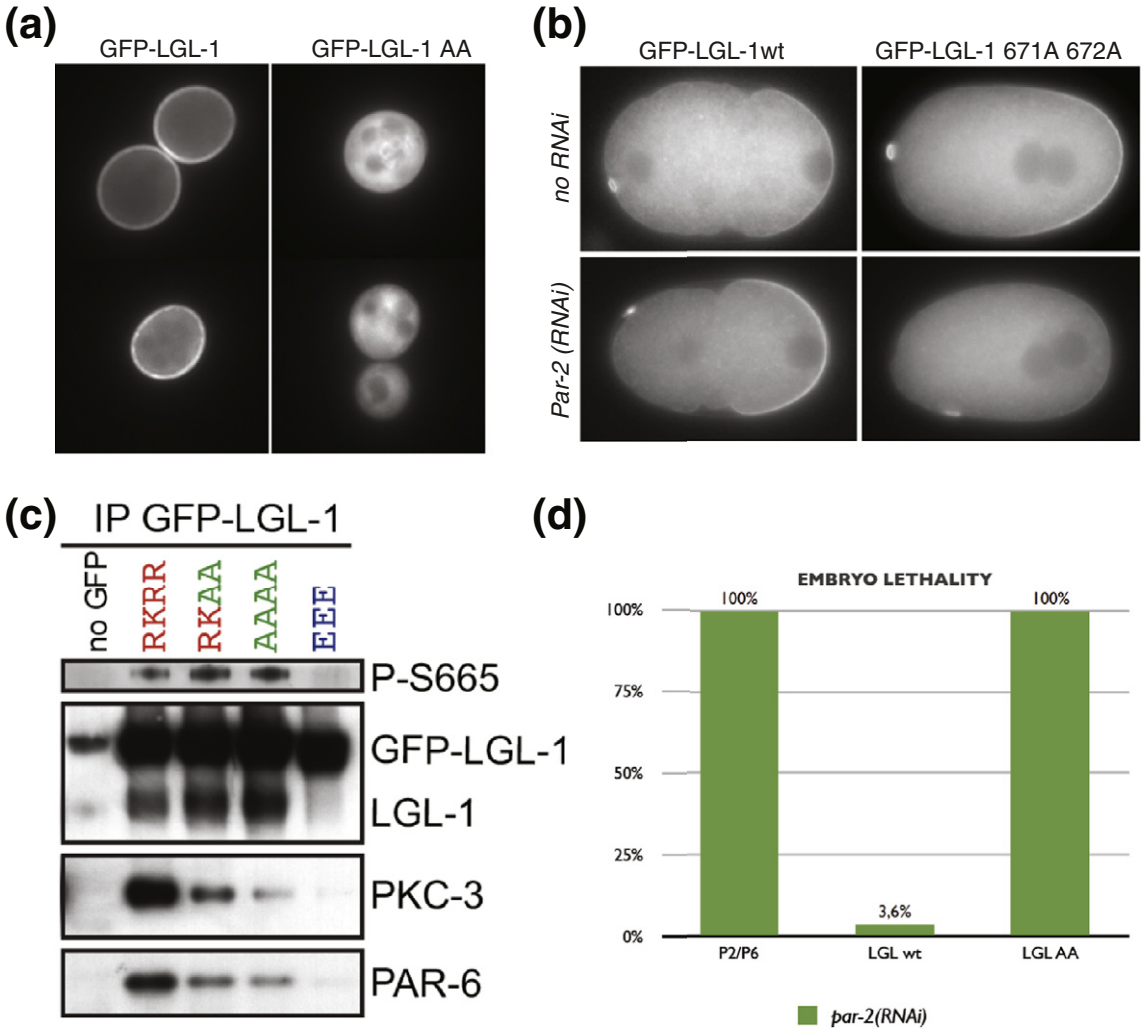

Fig. 6. LGL-1 arginines 671 and 672 are critical for LGL-1 function in yeast and *C. elegans* embryos. (a) GFP-LGL-1 WT but not an AA mutant 671A, 672A binds to the plasma membrane when expressed in yeast cells. (b) GFP-LGL-1 WT and AA mutant 671A, 672A localizes to the posterior cortex in control embryos (no RNAi condition, posterior is right). GFP-LGL-1 AA mutant loses membrane localization in par-2(RNAi) embryos, whereas GFP-LGL-1 WT localizes to the membrane and rescues par-2(RNAi) phenotype. (c) GFP-LGL-1 AA mutant (671A, 672A) and AAAA mutant (658A, 660A, 671A, 672A) show weaker interaction with PAR-6 and PKC-3 in immunoprecipitations (IP). Detection by LGL-1, PAR-6, PKC-3, and phosphoserine 665-specific antibodies. (d) GFP-LGL-1 WT but not the AA mutant 671A, 672A can rescue par-2(RNAi) embryo lethality when expressed in *C. elegans* embryos. P2/P6 is a transgenic line expressing GFP-PAR-2 and PAR-6-mcherry used as a control.

AAAA show weaker interactions with PAR-6 and PKC-3, indicating that mutations in the MBS not only affect membrane binding but also association with the anterior PARs PAR-6 and PKC-3 either directly or indirectly. Importantly, the LGL-1 mutants are still phosphorylated by PKC-3 *in vivo* (P-S665), indicating that the LGL-1 membrane binding mutations do not interfere with the PKC-3 phosphorylation sites (Fig. 6c).

Discussion

We reconstituted a functional LGL-1/aPKC polarity module in the form of a membrane switch in GUVs. In this system, a human aPKC co-encapsulated with the LGL-1 MBS peptide can be activated; thus, it phosphorylates LGL-1 MBS, inducing the detachment of the peptide from the vesicle inner membrane. This direct visualization of the phosphorylation-dependent LGL-1 MBS detachment, together with complementing experiments, indicates that the phosphorylation by PKC-3 regulates LGL-1 cortical localization, lowering dramatically its affinity for the plasma membrane.

In order to reconstitute LGL-1 in model membranes, we first had to elucidate the mechanism of the LGL-1 membrane binding. We identified a region (659–676) in the C-terminal LGL-specific domain, which is rich

in positively charged amino acids and can directly bind negatively charged membranes. Although the membrane binding takes place independent of what type of acidic lipid is used, LGL-1 shows the highest affinity for the diphosphoinositides PI(3,4)P2 and PI(4,5)P2, whose phosphate groups are located in two adjacent positions of the inositol ring. PI(4,5)P2 is the most abundant phosphoinositide of the inner leaflet of the plasma membrane and is normally targeted by phosphoinositide recognition domains with low headgroup specificity [26]. This finding might have a physiological relevance: the PI(4,5)P2-generating enzyme PPK-1 of *C. elegans* is in fact enriched in the posterior domain, where LGL-1 localizes [42]. However, there are no indications for an asymmetric localization of PI(3,4)P2 and PI(4,5)P2 in the *C. elegans* embryo yet, and quantitative studies of the lipid composition of the anterior and posterior plasma membrane of *C. elegans* embryos will be required.

Upon membrane binding, LGL-1 MBS folds into an alpha-helix, which forms three regions with distinct properties: (1) all basic amino acids align and form a positively charged patch; (2) the three amino acids that serve as phosphorylation sites for PKC-3 are located close to each other, creating a "switch" area; and (3) all remaining hydrophobic adjacent residues are probably buried in the membrane (Supplementary Material Fig. S9A). Interestingly, only mutations of specific basic amino acids of the positive patch interfere with the cortical localization of LGL-1 in yeast and in *C. elegans* embryos. A combined quadruple mutation of those residues lowers the affinity of LGL-1 MBS for PI(4,5)P2-containing membranes in our *in vitro* GUV binding assay, suggesting that the positions of the single basic amino acids in the LGL-1 MBS are important for their membrane binding specificity (Fig. 2d). The ionization behavior of the phosphoinositides is known to be linked to the specific position of the phosphate groups and, most importantly, to the ability of a protein to target a specific membrane environment [43].

The observation that LGL-1 binds the membrane through the same region that controls its cortex localization is partly consistent with the intramolecular auto-inhibition model proposed by Betschinger and colleagues [11]. Previously, it was assumed that LGL membrane association takes place through the N-terminal β-propeller domains. Although we cannot exclude that N-terminal parts of the proteins play a role in membrane binding *in vivo*, we did not identify N-terminal fragments in our yeast membrane binding screen. In addition, we do not have indications that the cell cortex contributes to LGL-1 binding, as treatment of the *C. elegans* embryos with cytochalasin or latrunculin does not remove LGL-1 from the membrane (data not shown). However, there might be additional protein binding partners on the membrane of the embryo.

Consistent with our results, Drosophila polarity proteins seem to be targeted to the cell cortex by binding to phospholipids as well [23].

When LGL-1 does not bind the membrane, its MBS has a random coil conformation and acts as a flexible hinge allowing the N and C termini of the protein to come together (Supplementary Material Fig. S10). This condition can be triggered or stabilized by PKC-dependent phosphorylation, with the phosphorylated LGL-1 having low membrane affinity. On the other hand, when LGL-1 binds the membrane, the MBS folds into an alpha-helix structure with reduced flexibility [44], eventually preventing the intramolecular association of the N and C termini of the protein and enabling interaction with other membrane-associated binding partners. In this condition, LGL-1 could be protected from the PKC-3 action, similar to PAR-2 [14], indicating that for LGL-1 activation/deactivation, phosphorylation might not be sufficient and another player could be involved in the LGL-1 cycle. One candidate could be PAR-6. Through its direct association with LGL-1 [12], it could enable PKC-3 to phosphorylate LGL-1 even in its membrane-bound state. PAR-6 is in fact known to activate aPKC through CDC-42 interaction [45].

How could LGL-1 regulate PAR domains in *C. elegans* embryos? In *par-2*-depleted embryos, GFP-LGL-1 is the sole posterior PAR component on the membrane, and we could imagine the following scenario in these embryos. At polarization, LGL-1 can enter the cell membrane, as anterior PARs are removed with the cortex flow, and a stable boundary of anterior PARs and LGL-1 is formed. At the posterior domain, LGL-1 is mostly inaccessible for phosphorylation, firstly, due to its membrane-binding-induced alpha-helix and, secondly, because anterior PARs cannot diffuse over long distances into the posterior domain [46]. However, at the domain boundary, LGL-1 encounters PAR-6, which is recruited by Cdc-42. Binding to PAR-6 could change LGL-1 conformation so that it becomes accessible for PKC-3 phosphorylation, which releases LGL-1 from binding to the membrane, and the whole PAR-6/PKC-3/LGL-1 complex is removed from the membrane at the PAR domain boundary. A membrane binding mutant of LGL-1 shows defects in membrane binding, but in addition, interaction with PAR-6/PKC-3 is weaker as well and the LGL-1 mutant is unable to maintain PAR domain boundaries. This could mean that LGL-1 phosphorylation is easier, as LGL-1 is less protected in the membrane. In addition, the weaker interaction of LGL-1 with PAR-6 and PKC-3 lowers its activity to remove PAR-6/PKC-3 from the membrane.

In conclusion, our results provide important molecular insights into the design features of the membrane switch forming the basis for PAR polarity induction. Although this is only the first step toward a full reconstitution of spontaneous polarity induction in a minimal system based on PAR-6 and LGL-1, it shows that important design parallels to other polarity and

pattern-forming systems involving a reversible membrane switch, such as the MinCDE system from *E. coli* [47]. We hypothesize that a similar role of the membrane as a catalytic template in symmetry-breaking processes will be revealed for many other essential morphogenetic processes in the future.

Materials and Methods

Materials

DOPC; DOPS; 1,2-dioleoyl-sn-glycero-3-phosphate (DOPA); 1,2-dioleoyl-sn-glycero-3-phospho-(1′-rac-Glycerol) (DOPG); L-α-phosphatidylinositol; cardiolipin (Heart, Bovine); 1,2-dioleoyl-sn-glycero-3-phosphoinositol-3-phosphate (PI(3)P); 1,2-dioleoyl-sn-glycero-3-phospho-(1′-myo-inositol-4′-phosphate) (PI(4)P); 1,2-dioleoyl-sn-glycero-3-phospho-(1′-myo-inositol-5′-phosphate) (PI(5)P); 1,2-dioleoyl-sn-glycero-3-phospho-(1′-myo-Inositol-3′,4′-bisphosphate) (PI(3,4)P2); 1,2-dioleoyl-sn-glycero-3-phospho-(1′-myo-Inositol-3′,5′-bisphosphate) (PI(3,5)P2); PI(4,5)P2; 1,2-dioleoyl-sn-glycero-3-phospho-(1′-myo-inositol-3′,4′,5′-trisphosphate) (PI(3,4,5)P3) and L-α-phosphatidylinositol-4,5-bisphosphate (bPI(4,5)P2), and 1,2-di-(9Z-octadecenoyl)-sn-glycero-3-[(*N*-(5-amino-1-carboxypentyl)iminodiacetic acid)succinyl] (DGS-NTA(Ni)) were purchased from Avanti Polar Lipids, Inc. (Alabaster, AL). Atto488 NHS-Ester was purchased from ATTO-TEC GmbH (Siegen, Germany). Texas Red 1,2-dihexadecanoyl-sn-glycero-3-phosphoethanolamine, triethylammonium salt (Texas Red DHPE) was purchased from Life Technologies Corporation (Carlsbad, CA). Active recombinant human PKC-ζ was purchased from Merck Millipore (Billerica, MA). [γ-32P]ATP was purchased from PerkinElmer (Waltham, MA). Alpha-hemolysin (powder) from *Staphylococcus aureus*, bovine serum albumin (BSA), mineral oil, Ficoll PM 70, and 2,2,2-TFE were purchased from Sigma-Aldrich (St. Louis, MO). The pGEX-6P-1 vector, GSTrap HP 1-mL column, HisTrap HP 1-mL column, and PreScission Protease were purchased from GE Healthcare (Little Chalfont, UK). Reducing Agent Compatible bicinchoninic acid Protein Assay was purchased from Thermo Fisher Scientific (Waltham, MA). All solvent used were of Uvasol spectroscopic grade.

Protonation of phosphoinositides using acid

All phoshoinositides were protonated to enhance their incorporation into liposomes. The protonation protocol was developed by Olga Perisic (MRC Laboratory of Molecular Biology, Cambridge, UK) and used with minor modification. Briefly, lyophilized phoshoinositides were resuspended at 2.5 mM final concentration in subsequent steps with different solvent mixtures: (1) chloroform; (2) 2:1:0.01 (vol:vol:vol) mixture of chloroform, methanol, and hydrochloric acid 1 N; (3) 3:1 (vol:vol) mixture of chloroform and methanol; and (4) chloroform. After each step, the lipid solution was dried 15 min under N_2; after step (1) and (2), the solution was additionally dried for 1 h under vacuum. In step (2), the lipid solution was incubated 15 min before drying. The lipid film was finally resuspended in chloroform at 1 mM final concentration and stored at −20 °C for a few months.

LGL-1 expression and purification

LGL-1 5/6 (aa 469–702) was cloned into a pGEX-6P-1 vector in which eGFP-His6 was previously cloned using the restriction enzymes BamHI and NotI [48]. The LGL-1 mutants S661A/S665A/T669A (AAA), S661E/S665E/T669E (EEE), and R658A/K660A/RR671AA (AAAA) were generated with the QuikChangeLightning Site-Directed Mutagenesis Kit (Agilent Technologies, Santa Clara, CA) according to the manufacturer's instructions. All clones were expressed in the *E. coli* strain BL21(DE3). The proteins were purified in the presence of 1% Triton X-100 using GSTrap HP columns, followed by direct cleavage of the glutathione *S*-transferase tag with PreScission Protease on column and a second purification step with a HisTrap HP column according to the manufacturer's instructions. Protein concentrations were determined using the bicinchoninic acid protein assay. Purified LGL-1 5/6 was precleared at 120,000*g* for 30 min at 4 °C in a MLA-130 rotor (Beckman Coulter, Pasadena, CA) and was stored at −80 °C in the presence of 10% glycerol.

LGL-1 MBS peptide synthesis and labeling

The LGL-1 MBS WT (G5EEI1_CAEEL 656–681, acetyl-FQRFKSLKKSLRKTFRRKKKGTETLM-amide) and EEE peptide (acetyl-FQRFKELKKELRKEFRRKKKGTETLM-amide) were synthesized using Fmoc chemistry and purified to >90% by preparative RP-HPLC. For imaging experiments, the peptides were labeled by coupling Atto488 NHS-Ester at the N terminus. Purity and identity of the peptides were checked by analytical RP-HPLC and electrospray mass spectrometry. Both peptides were stored at −80 °C and lyophilized or in water at 1 mg/mL final concentration.

In vitro LGL-1 phosphorylation by human PKC-ζ

In vitro phosphorylation was performed similarly as described before [14] with the following modifications. We incubated 5.0 μM LGL-1 MBS WT and EEE peptides with 1 nM recombinant human PKC-ζ in kinase buffer [20 mM Hepes (pH 7.4), 5 mM $MgCl_2$, and 1 mM DTT] containing 60 μM cold ATP and 1.315 μCi [γ-32P]ATP at room temperature (RT). Kinase reactions were carried out by incubating samples on ice (for time 0 samples) or at 30 °C and were terminated by adding 5X Laemmli loading buffer at different time points (10, 20, 30, 40, and 50 min). Proteins were separated by a handcast 18% Tris–glycine gel, stained with Coomassie, and fixed and dried on 1.5-mm filter paper. The dried gels were exposed to radiographic films at RT ON and digitalized with a LAS-3000 (Fujifilm, Tokyo, Japan), exposing them for 1–8 s on a DIA tray. The autoradiographs were analyzed with the gel analysis tool of Fiji[‡]. LGL-1 MBS WT phosphorylated for 50 min was included in every gel and used as a reference to normalize the amount of phosphorylation.

SLB formation

SLBs were prepared directly on glass using the vesicle fusion method [49] as described before for freshly cleaved mica [50]. Pure DOPC or DOPC doped with either 20%mol DOPS or 7.5%mol bPI(4,5)P2 was used as lipid mixtures.

SLB formation was performed at least 10 °C above the highest transition temperature of the lipid used. When the temperature used was higher than RT, the samples were slowly cooled down before further usage. SLBs were imaged, and fluorescence recovery after photobleaching was recorded to assess the correct formation of the bilayer.

GUV formation using platinum wires

GUVs were prepared in homemade teflon and platinum (Pt) chambers as previously described with minor modifications [51]. Lipid stock solutions were prepared by dissolving lyophilized lipids into chloroform at a final concentration of 1 mg/mL and were either used immediately or stored at −20 °C up to a few months. When frozen, the lipid stock solutions were allowed to warm to RT before usage. Then, 6 µL of the lipid solution was spread uniformly on the Pt wires and dried under vacuum at RT for 1 h to allow complete evaporation of the solvents. Vesicles were formed using the electroformation method [52] with 2 V and 10 Hz for a minimum of 90 min in a water solution of sucrose matching the osmolarity of the working buffer used for the following experiments. The frequency was then decreased to 2 Hz for ca 15–30 min, so that the GUVs formed gently detach from the Pt wires. Electroformation was performed at least 10 °C above the highest transition temperature of the lipid used. When the temperature used was higher than RT, the samples were slowly cooled down. After electroformation, the GUVs were diluted in working buffer and transferred to an observation chamber (Nunc Lab-Tek II chambered coverglass; Thermo Fisher Scientific) previously passivated with a 2 mg/mL BSA solution for at least 30 min and rinsed with water and working buffer.

GUV formation using the droplet transfer method

GUVs were prepared as previously described [38–40] with minor modifications. Lipids were first mixed in a glass vial rinsed with acetone and chloroform and dried 15 min under N_2 and 1 h under vacuum. The lipid film was then dissolved in 5 or 10 mL of mineral oil at a final concentration of 0.5 mg/mL and was sonicated in a bath at RT for 20 min (Bransonic Ultrasonic Cleaners Model 2510, Branson Ultrasonics, Danbury, CT). The oil–lipid mixture was either used immediately or stored at 4 °C up to 1 week. Before each usage, the oil–lipid mixture was allowed to warm to RT and was sonicated at RT for 5 min. Then, 500 µL of the outer buffer [20 mM Hepes (pH 7.4), 5 mM $MgCl_2$, 100 mM glucose, and 1 mM DTT] was placed in a 2-mL tube, overlaid with 500 µL of the oil–lipid mixture, and incubated for at least 2 h at RT to allow a lipid monolayer to assemble at the interface. We added 15 µL of the internal solution [kinase reactions at 1:5 dilution in internal buffer: 20 mM Hepes (pH 7.4), 5 mM $MgCl_2$, 100 mM sucrose, 1 mM DTT, and 50 g/L Ficoll PM 70] to 500 µL of the oil–lipid mixture and we suspended it by gentle pipetting back and forth until a cloudy emulsion was obtained. The whole volume of the emulsion was then slowly poured on top of the oil–lipid mixture, thus resulting in a three-level sample with the outer buffer at the bottom, the oil–lipid mixture in the middle, and the emulsion on top. The tube was then centrifuged in two subsequent steps (10 min at 100*g*, 10 min at 350*g*), in which emulsion drops of different size passed through the lipid monolayer to form GUVs filled with the internal solution and surrounded by the outer buffer. The outer buffer containing the GUVs was gently collected and transferred to an observation chamber previously passivated with a 2 mg/mL BSA solution for at least 30 min and rinsed with water and outer buffer.

SUV formation and CD spectroscopy

DOPC alone or mixed with negatively charged lipids at the desired molar ratio in chloroform was dried 15 min under N_2 and 1 h under vacuum. The dried lipids were rehydrated in CD buffer [1 mM NaH_2PO_4 and 50 mM NaF (pH 7.4)] to a final concentration of 10 mg/mL, vortexes for 5 min and bath sonicated until the solution became clear. SUV formation was performed at least 10 °C above the highest transition temperature of the lipid used. When the temperature used was higher than RT, the samples were slowly cooled down before further usage. SUVs were used for experiments on the day they were prepared. Far-UV CD spectra were acquired at 25 °C on a Jasco J-715 spectropolarimeter (Jasco, Easton, MD) as previously described [53,54]. The unlabeled LGL-1 MBS peptide concentration was kept at 50 µM and mixed with different amount of SUVs (1:10, 1:50, and 1:100 M ratio) in CD buffer. Eight scans were accumulated, and background signal (buffer only and lipid only) was subtracted from the spectra. The alpha-helix content of the peptide in the presence of different lipid mixtures was estimated from the CD spectra with the CDPro software package[§] using the CONTIN method and the SMP56 protein set. CD spectra of the peptide in the absence of lipids in TFE were acquired and used to normalize the alpha-helix content of the peptide.

LUV formation, dynamic light scattering (DLS), and zeta-potential measurements

DOPC alone or mixed with negatively charged lipids at the desired molar ratio in chloroform was dried 15 min under N_2 and 1 h under vacuum. After solvent evaporation, the lipid film was rehydrated in SLB buffer [150 mM NaCl and 10 mM Hepes (pH 7.4)] at 1 mg/mL lipid concentration and resuspended by vortexing. The vesicle suspension was then subjected to 8 freeze–thaw cycles and extruded 21 times through a 100-nm polycarbonate membrane. After extrusion, LUVs were diluted to a final concentration of 100 µM, filtered with a 0.45-µm mixed cellulose esters filter, and aliquoted. Each aliquot was incubated with none or different amounts of the LGL-1 MBS peptide (0, 0.5, 1, 2, 4, 6, and 8 µM) for 15 min at RT. DLS and zeta-potential measurements were performed with a Malvern Zetasizer Nano ZSP system (Malvern, UK) as previously described with minor modifications [29]. Ultra-micro UV-transparent spectrophotometry cuvettes (Brand, Essex, CT) and disposable folded capillary cells DTS 1070 (Malvern, Malvern, UK) were used in DLS and zeta-potential measurements, respectively. For DLS experiments, 2 scans (13 runs each) were performed at 25 °C with an initial equilibration time of 5 min. For zeta-potential measurements, 15 scans (20–100 runs each) were performed at 25 °C with a constant voltage of 40 mV and an initial equilibration time of 5 min. After each scan, the instrument paused for 90 s and every 5 scans for 5 min. Values of the viscosity and refractive index were set at 0.8882 cP and 1.330, respectively. Experiments were performed in duplicate. The zeta-potential values obtained from the instrument software were plotted

against the peptide concentration and fit to Eq. (4) of ref. [32]. The fitting was performed using SigmaPlot 12.3 (Systat Software, Inc., San Jose, CA). Care was taken to ensure that no vesicle aggregation took place in the peptide concentration range used during the measurements. For this reason, the particle size was checked with DLS before and after the addition of the peptide (Supplementary Material Fig. S2A) and at the end of the measurement runs. The particle size and PdI increase with higher LGL-1 MBS concentrations (Supplementary Material Table S3), due to the increasing amount of peptide bound to the vesicles and the presence of vesicles with different amounts of peptide bound, respectively.

LGL-1 fragment generation

For the selection of PCR reactions, each of the 8 individual LGL-1 forward oligos was combined with 1 of the 8 individual reverse oligos to generate 36 different LGL-1 PCR fragments of different lengths (e.g., 1/1, 1/2, 1/3,…..2/2, 2/3, 2/4,…; Supplementary Material Fig. S11). PCR was done in duplicates, except for 8 fragments with identical oligo number (e.g., 1/1, 2/2…), to give a total of 64 = (36 × 2)− 8 PCR reactions. PCR products were verified by gel analysis and purified for further yeast transformation.

Yeast membrane binding assays and *in vivo* localization

Membrane binding was tested in yeast by fusing LGL-1 fragments to active Ras [55]. LGL-1 fragments (see above) were amplified with 5′ nucleotide overhangs homologous to the p3SOBL2 vector used for the expression of activated Ras. For recombination cloning, the LGL-1 fragments and the BamHI/XhoI-digested vector p3SOBL2 were transformed into cdc25ts yeast cells by standard transformation procedures [56]. Membrane binding was tested by spotting transformed yeast cells in dilution series onto plates and growing them for 3–5 days at 23 °C and 37 °C. Mutations of residues in the membrane binding region were introduced by Quikchange mutagenesis (Agilent) and verified by DNA sequencing. GFP-LGL-1 WT or the AA mutant R671A, R672A protein was expressed from a 2-μ plasmid pGO-GFP (Addgene) in BY4742 yeast cells (Euroscarf).

C. elegans techniques and lines

Worms were grown and maintained as described [57]. RNA interference (RNAi) was done by the feeding method [58]. Worms were kept on feeding plates for at least 24 h at 25 °C before analysis. Worm lines TH270 (GFP-LGL-1 WT), CH190 (GFP-LGL-1 R671A, R672A), and CH191 (GFP-LGL-1 R658A, K660A, R671A, R672A) expressing LGL-1 WT and mutant from a pie-1 promoter and terminator were used and made by particle bombardment using unc-119 rescue [59]. For assaying embryo lethality, par-2(RNAi) was done for 27 h at 25 °C, with each 4 worms placed on three different NGM plates and allowed to lay eggs for 4.5 h. Embryos and L1 larvae were counted the next day, and embryo lethality was averaged from the three plates.

Immunoprecipitation from *C. elegans* embryos

Worms were grown synchronously on peptone plates. Embryos were harvested by bleaching worms in 200 mM NaOH and 20% NaClO solution (Merck) for 8 min with vortexing. Purified embryos were washed in M9 buffer and frozen in liquid nitrogen. Then, 0.5 g of embryos of each worm line was used for immunoprecipitation as described previously [7]. Briefly, embryo extracts were prepared by sonication in H100 buffer containing 0.2% Triton X-100 and 10% glycerol and cleared by centrifugation at 230,000*g* for 30 min, and immunocomplexes were purified with anti-GFP antibodies raised in goats coupled to magnetic protein G beads (Invitrogen). Phosphorylated S665 was detected by a phospho-specific and affinity-purified antibody raised in rabbits from the peptide H2N-KSLKKS(P03H2)LRKTFRC-COOH (Eurogentec).

Microscopy, image processing, and analysis

Fluorescence confocal imaging of GUVs and SLBs was performed on a LSM 780 ConfoCor3 system (Carl Zeiss, Jena, Germany) using a C-Apochromat 40×/1.2 W Corr M27 objective. Sample was excited either by a 488-nm (green channel; e.g., eGFP, Atto488) and/or a 561-nm (orange channel; e.g., Texas Red DHPE) laser. The fluorescence was then collected through 493–543-nm and 569–630-nm band-pass filters, respectively, with a 40-μm pinhole. Fluorescence confocal images were processed and analyzed with Fiji[‖]. When needed, image contrast was enhanced through normalization. The binding of the labeled LGL-1 5/6 WT and EEE mutant was determined from the peaks of the intensity radial profile plots of confocal images taken at GUV's equator using the radial profile angle plug-in[¶]. The binding of the labeled LGL-1 5/6 WT and AAAA mutant was determined from intensity profiles of confocal z-stack images taken parallel at the SLBs' plane using the z-project function. LGL-1 fluorescence intensity values were background corrected, averaged, and normalized by the value obtained in SLBs containing DOPC only. Yeast cells were imaged with a DeltaVision RT imaging system (Applied Precision, LLC; IX70 Olympus) equipped with a charge-coupled device camera (CoolSNAP HQ; Roper Scientific) using an Olympus 1003 1.40 NA UPlanSApo lens. Live imaging of fluorescent worm lines was on a Zeiss Axioplan II Widefield microscope with a Zeiss 633 1.4 Apochromat lens and a Hamamatsu Orca ER 12-bit camera.

Statistical analysis

Statistical analysis was performed using SigmaPlot 12.3. When the means of the two sets of data were compared (Figs. 2d and 4d), a *t*-test was used and two-tailed *p*-values were reported. Comparison of more than two sets of data (Fig. 1g) was carried out with one-way ANOVA. To isolate the group or groups that differ from the others, ANOVA was followed up with an all-pairwise multiple comparison procedure (Holm–Šidák Method). The level of alpha was kept at 0.05 for all statistical analyses.

Acknowledgments

We thank Sigrid Bauer and Lisa Tübel for invaluable technical assistance; and Elisabeth Weyher-Stingl, Stefan Pettera, and Dr. Stephan Uebel of the MPI-B core facility for helping with CD measurements and for

synthesizing and labeling the LGL-1 MBS peptides, respectively. This project was funded through the MaxSynBio network of the MPG/BMBF.

Appendix A. Supplementary Data

Supplementary data to this article can be found online at http://dx.doi.org/10.1016/j.jmb.2016.10.003.

Received 18 July 2016;
Received in revised form 28 September 2016;
Accepted 1 October 2016
Available online 6 October 2016

Keywords:
cell polarity;
lethal giant larvae (LGL);
synthetic biology;
giant unilamellar vesicles;
C. elegans

Present address: I. Visco, Max Planck Institute for Molecular Physiology, Otto-Hahn-Str. 11, 44227 Dortmund, Germany.
†I.V. and C.H. contributed equally to this work.
‡http://rsb.info.nih.gov/ij/docs/menus/analyze.html#gels
§http://lamar.colostate.edu/~sreeram/CDPro/
||http://fiji.sc/Fiji
¶http://rsbweb.nih.gov/ij/plugins/radial-profile.html

Abbreviations used:
aPKC, atypical protein kinase C; bPI(4,5)P2, L-α-phosphatidylinositol-4,5-bisphosphate; BSA, bovine serum albumin; DGS-NTA(Ni), 1,2-di-(9Z-octadecenoyl)-sn-glycero-3-[(*N*-(5-amino-1-carboxypentyl)iminodiacetic acid) succinyl]; DLS, dynamic light scattering; DOPC, 1,2-dioleoyl-sn-glycero-3-phosphocholine; DOPS, 1,2-di-(9Z-octadecenoyl)-sn-glycero-3-phospho-L-serine; eGFP, enhanced green fluorescent protein; GFP, green fluorescent protein; GUV, giant unilamellar vesicle; His6, hexahistidine tag; LUVs, large unilamellar vesicles; LGL-1, lethal giant larvae 1; MBS, membrane binding sequence; PAR, partitioning-defective proteins; PI(4,5)P2, 1,2-dioleoyl-sn-glycero-3-phospho-(1′-myo-inositol-4′,5′-bisphosphate); PKC, protein kinase C; Pt, platinum; RNAi, RNA interference; RT, room temperature; SUVs, small unilamellar vesicles; SLBs, supported lipid bilayers; TFE, trifluoroethanol; WT, wild type.

References

[1] A.H. Chau, J.M. Walter, J. Gerardin, C. Tang, W.A. Lim, Designing synthetic regulatory networks capable of self-organizing cell polarization, Cell 151 (2012) 320–332, http://dx.doi.org/10.1016/j.cell.2012.08.040.
[2] H. Meinhardt, Turing's theory of morphogenesis of 1952 and the subsequent discovery of the crucial role of local self-enhancement and long-range inhibition, Interface Focus 2 (2012) 407, http://dx.doi.org/10.1098/rsfs.2011.0097.
[3] S.J. Altschuler, S.B. Angenent, Y. Wang, L.F. Wu, On the spontaneous emergence of cell polarity, Nature 454 (2008) 886–889, http://dx.doi.org/10.1038/nature07119.
[4] B.D. Slaughter, S.E. Smith, R. Li, Symmetry breaking in the life cycle of the budding yeast, Cold Spring Harb. Perspect. Biol. 1 (2009) a003384, http://dx.doi.org/10.1101/cshperspect.a003384.
[5] F. Motegi, G. Seydoux, The PAR network: redundancy and robustness in a symmetry-breaking system, Philos. Trans. R. Soc. Lond. Ser. B Biol. Sci. 368 (2013) 20,130,010, http://dx.doi.org/10.1098/rstb.2013.0010.
[6] C. Hoege, A.A. Hyman, Principles of PAR polarity in *Caenorhabditis elegans* embryos, Nat. Rev. Mol. Cell Biol. 14 (2013) 315–322, http://dx.doi.org/10.1038/nrm3558.
[7] C. Hoege, A.-T. Constantinescu, A. Schwager, N.W. Goehring, P. Kumar, A.A. Hyman, LGL can partition the cortex of one-cell *Caenorhabditis elegans* embryos into two domains, Curr. Biol. 20 (2010) 1296–1303, http://dx.doi.org/10.1016/j.cub.2010.05.061.
[8] A. Beatty, D.G. Morton, K. Kemphues, The *C. elegans* homolog of *Drosophila* lethal giant larvae functions redundantly with PAR-2 to maintain polarity in the early embryo, Development 137 (2010) 3995–4004, http://dx.doi.org/10.1242/dev.056028.
[9] A.N. Ndifon, Variations of developmental events, *skn-1* and *pie-1* expression, and gene regulatory networks in nematodes with different modes of reproduction, (2013) 1–132.
[10] V. Vasioukhin, Lethal giant puzzle of Lgl, Dev. Neurosci. 28 (2006) 13–24, http://dx.doi.org/10.1159/000090749.
[11] J. Betschinger, F. Eisenhaber, J.A. Knoblich, Phosphorylation-induced autoinhibition regulates the cytoskeletal protein lethal (2) giant larvae, Curr. Biol. 15 (2005) 276–282, http://dx.doi.org/10.1016/j.cub.2005.01.012.
[12] P.J. Plant, J.P. Fawcett, D. Lin, A.D. Holdorf, K. Binns, S. Kulkarni, et al., A polarity complex of mPar-6 and atypical PKC binds, phosphorylates and regulates mammalian Lgl, Nat. Cell Biol. 5 (2003) 301–308, http://dx.doi.org/10.1038/ncb948.
[13] L. Boyd, S. Guo, D. Levitan, D.T. Stinchcomb, K.J. Kemphues, PAR-2 is asymmetrically distributed and promotes association of P granules and PAR-1 with the cortex in *C. elegans* embryos, Development 122 (1996) 3075–3084.
[14] F. Motegi, S. Zonies, Y. Hao, A.A. Cuenca, E. Griffin, G. Seydoux, Microtubules induce self-organization of polarized PAR domains in *Caenorhabditis elegans* zygotes, Nat. Cell Biol. 13 (2011) 1361–1367, http://dx.doi.org/10.1038/ncb2354.
[15] R. Benton, D.S. Johnston, *Drosophila* PAR-1 and 14-3-3 inhibit Bazooka/PAR-3 to establish complementary cortical domains in polarized cells, Cell 115 (2003) 691–704.
[16] B. Li, H. Kim, M. Beers, K. Kemphues, Different domains of *C. elegans* PAR-3 are required at different times in development, Dev. Biol. 344 (2010) 745–757, http://dx.doi.org/10.1016/j.ydbio.2010.05.506.
[17] E. Morais-de-Sá, V. Mirouse, D.S. Johnston, aPKC phosphorylation of Bazooka defines the apical/lateral border in *Drosophila* epithelial cells, Cell 141 (2010) 509–523, http://dx.doi.org/10.1016/j.cell.2010.02.040.
[18] A. Beatty, D.G. Morton, K. Kemphues, PAR-2, LGL-1 and the CDC-42 GAP CHIN-1 act in distinct pathways to maintain polarity in the *C. elegans* embryo, Development 140 (2013) 2005–2014, http://dx.doi.org/10.1242/dev.088310.
[19] M.P. Krahn, D.R. Klopfenstein, N. Fischer, A. Wodarz, Membrane targeting of Bazooka/PAR-3 is mediated by direct binding to phosphoinositide lipids, Curr. Biol. 1–7 (2010), http://dx.doi.org/10.1016/j.cub.2010.01.065.

[20] K. Moravcevic, J.M. Mendrola, K.R. Schmitz, Y.-H. Wang, D. Slochower, P.A. Janmey, et al., Kinase associated-1 domains drive MARK/PAR1 kinases to membrane targets by binding acidic phospholipids, Cell 143 (2010) 966–977, http://dx.doi.org/10.1016/j.cell.2010.11.028.

[21] Y. Hao, L. Boyd, G. Seydoux, Stabilization of cell polarity by the *C. elegans* RING protein PAR-2, Dev. Cell 10 (2006) 199–208, http://dx.doi.org/10.1016/j.devcel.2005.12.015.

[22] W. Dong, X. Zhang, W. Liu, Y.-J. Chen, J. Huang, E. Austin, et al., A conserved polybasic domain mediates plasma membrane targeting of Lgl and its regulation by hypoxia, J. Cell Biol. 211 (2015) 273–286, http://dx.doi.org/10.1083/jcb.201503067.

[23] M.J. Bailey, K.E. Prehoda, Establishment of Par-Polarized Cortical Domains via Phosphoregulated Membrane Motifs, Dev. Cell 35 (2015) 199–210, http://dx.doi.org/10.1016/j.devcel.2015.09.016.

[24] K. Carvalho, L. Ramos, C. Roy, C. Picart, Giant unilamellar vesicles containing phosphatidylinositol(4,5)bisphosphate: characterization and functionality, Biophys. J. 95 (2008) 4348–4360, http://dx.doi.org/10.1529/biophysj.107.126912.

[25] L. Schmitt, C. Dietrich, R. Tampe, Synthesis and characterization of chelator-lipids for reversible immobilization of engineered proteins at self-assembled lipid interfaces, J. Am. Chem. Soc. 116 (1994) 8485–8491.

[26] M.A. Lemmon, Membrane recognition by phospholipid-binding domains, Nat. Rev. Mol. Cell Biol. 9 (2008) 99–111, http://dx.doi.org/10.1038/nrm2328.

[27] M.A. Lemmon, Phosphoinositide recognition domains, Traffic 4 (2003) 201–213.

[28] S. McLaughlin, J. Wang, A. Gambhir, D. Murray, PIP_2 and proteins: interactions, organization, and information flow, Annu. Rev. Biophys. Biomol. Struct. 31 (2002) 151–175, http://dx.doi.org/10.1146/annurev.biophys.31.082901.134259.

[29] J.M. Freire, M.M. Domingues, J. Matos, M.N. Melo, A.S. Veiga, N.C. Santos, et al., Using zeta-potential measurements to quantify peptide partition to lipid membranes, Eur. Biophys. J. 40 (2011) 481–487, http://dx.doi.org/10.1007/s00249-010-0661-4.

[30] S.H. Brewer, W.R. Glomm, M.C. Johnson, M.K. Knag, S. Franzen, Probing BSA binding to citrate-coated gold nanoparticles and surfaces, Langmuir 21 (2005) 9303–9307, http://dx.doi.org/10.1021/la050588t.

[31] E.D. Kaufman, J. Belyea, M.C. Johnson, Z.M. Nicholson, J.L. Ricks, P.K. Shah, et al., Probing protein adsorption onto mercaptoundecanoic acid stabilized gold nanoparticles and surfaces by quartz crystal microbalance and ζ-potential measurements, Langmuir 23 (2007) 6053–6062, http://dx.doi.org/10.1021/la063725a.

[32] H.G. Franquelim, A.S. Veiga, G. Weissmüller, N.C. Santos, M.A.R.B. Castanho, Unravelling the molecular basis of the selectivity of the HIV-1 fusion inhibitor sifuvirtide towards phosphatidylcholine-rich rigid membranes, Biochim. Biophys. Acta 1798 (2010) 1234–1243, http://dx.doi.org/10.1016/j.bbamem.2010.02.010.

[33] A.S. Ladokhin, M. Fernández-Vidal, S.H. White, CD spectroscopy of peptides and proteins bound to large unilamellar vesicles, J. Membr. Biol. 236 (2010) 247–253, http://dx.doi.org/10.1007/s00232-010-9291-0.

[34] P. Luo, R.L. Baldwin, Mechanism of helix induction by trifluoroethanol: a framework for extrapolating the helix-forming properties of peptides from trifluoroethanol/water mixtures back to water, Biochemistry 36 (1997) 8413–8421, http://dx.doi.org/10.1021/bi9707133.

[35] S.H. White, W.C. Wimley, A.S. Ladokhin, K. Hristova, Protein folding in membranes: determining energetics of peptide–bilayer interactions, Methods Enzymol. 295 (1998) 62–87.

[36] A. Gambhir, G. Hangyás-Mihályné, I. Zaitseva, D.S. Cafiso, J.Y. Wang, D. Murray, et al., Electrostatic sequestration of PIP2 on phospholipid membranes by basic/aromatic regions of proteins, Biophys. J. 86 (2004) 2188–2207, http://dx.doi.org/10.1016/S0006-3495(04)74278-2.

[37] J. Betschinger, K. Mechtler, J.A. Knoblich, The Par complex directs asymmetric cell division by phosphorylating the cytoskeletal protein Lgl, Nature 422 (2003) 326–330, http://dx.doi.org/10.1038/nature01486.

[38] S. Pautot, B.J. Frisken, D.A. Weitz, Production of unilamellar vesicles using an inverted emulsion, Langmuir 19 (2003) 2870–2879, http://dx.doi.org/10.1021/la026100v.

[39] L.-L. Pontani, J. van der Gucht, G. Salbreux, J. Heuvingh, J.-F. Joanny, C. Sykes, Reconstitution of an actin cortex inside a liposome, Biophys. J. 96 (2009) 192–198, http://dx.doi.org/10.1016/j.bpj.2008.09.029.

[40] E.J. Cabre, A. Sanchez-Gorostiaga, P. Carrara, N. Ropero, M. Casanova, P. Palacios, et al., Bacterial division proteins FtsZ and ZipA induce vesicle shrinkage and cell membrane invagination, J. Biol. Chem. 288 (2013) 26,625–26,634, http://dx.doi.org/10.1074/jbc.M113.491688.

[41] D.L. Richmond, E.M. Schmid, S. Martens, J.C. Stachowiak, N. Liska, D.A. Fletcher, Forming giant vesicles with controlled membrane composition, asymmetry, and contents, Proc. Natl. Acad. Sci. U. S. A. 108 (2011) 9431–9436, http://dx.doi.org/10.1073/pnas.1016410108.

[42] C. Panbianco, D. Weinkove, E. Zanin, D. Jones, N. Divecha, M. Gotta, et al., A casein kinase 1 and PAR proteins regulate asymmetry of a PIP2 synthesis enzyme for asymmetric spindle positioning, Dev. Cell 15 (2008) 198–208, http://dx.doi.org/10.1016/j.devcel.2008.06.002.

[43] E.E. Kooijman, K.E. King, M. Gangoda, A. Gericke, Ionization properties of phosphatidylinositol polyphosphates in mixed model membranes, Biochemistry 48 (2009) 9360–9371, http://dx.doi.org/10.1021/bi9008616.

[44] E.G. Emberly, R. Mukhopadhyay, N.S. Wingreen, C. Tang, Flexibility of α-helices: results of a statistical analysis of database protein structures, J. Mol. Biol. 327 (2003) 229–237, http://dx.doi.org/10.1016/S0022-2836(03)00097-4.

[45] T. Yamanaka, Y. Horikoshi, A. Suzuki, Y. Sugiyama, K. Kitamura, R. Maniwa, et al., PAR-6 regulates aPKC activity in a novel way and mediates cell–cell contact-induced formation of the epithelial junctional complex, Genes Cells 6 (2001) 721–731.

[46] N.W. Goehring, C. Hoege, S.W. Grill, A.A. Hyman, PAR proteins diffuse freely across the anterior–posterior boundary in polarized *C. elegans* embryos, J. Cell Biol. 193 (2011) 583–594, http://dx.doi.org/10.1083/jcb.201011094.

[47] M. Loose, K. Kruse, P. Schwille, Protein self-organization: lessons from the min system, Annu. Rev. Biophys. 40 (2011) 315–336, http://dx.doi.org/10.1146/annurev-biophys-042910-155332.

[48] F.A. Thomas, I. Visco, Z. Petrášek, F. Heinemann, P. Schwille, Introducing a fluorescence-based standard to quantify protein partitioning into membranes, Biochim. Biophys. Acta 1848 (2015) 2932–2941, http://dx.doi.org/10.1016/j.bbamem.2015.09.001.

[49] A.A. Brian, H.M. McConnell, Allogeneic stimulation of cytotoxic T cells by supported planar membranes, Proc. Natl. Acad. Sci. U. S. A. 81 (1984) 6159–6163.

[50] I. Visco, S. Chiantia, P. Schwille, Asymmetric supported lipid bilayer formation via methyl-β-cyclodextrin mediated lipid

exchange: influence of asymmetry on lipid dynamics and phase behavior, Langmuir 30 (2014) 7475–7484, http://dx.doi.org/10.1021/la500468r.

[51] A.J. García-Sáez, D.C. Carrer, P. Schwille, Fluorescence correlation spectroscopy for the study of membrane dynamics and organization in giant unilamellar vesicles, Methods Mol. Biol. 606 (2010) 493–508, http://dx.doi.org/10.1007/978-1-60761-447-0_33.

[52] M.I. Angelova, D.S. Dimitrov, Liposome electroformation, Faraday Discuss. 81 (1986) 303, http://dx.doi.org/10.1039/dc9868100303.

[53] T.H. Szeto, S.L. Rowland, L.I. Rothfield, G.F. King, Membrane localization of MinD is mediated by a C-terminal motif that is conserved across eubacteria, archaea, and chloroplasts, Proc. Natl. Acad. Sci. U. S. A. 99 (2002) 15,693–15,698, http://dx.doi.org/10.1073/pnas.232590599.

[54] T.H. Szeto, S.L. Rowland, C.L. Habrukowich, G.F. King, The MinD membrane targeting sequence is a transplantable lipid-binding helix, J. Biol. Chem. 278 (2003) 40,050–40,056, http://dx.doi.org/10.1074/jbc.M306876200.

[55] S.J. Isakoff, T. Cardozo, J. Andreev, Z. LI, K.M. Ferguson, R. Abagyan, et al., Identification and analysis of PH domain-containing targets of phosphatidylinositol 3-kinase using a novel *in vivo* assay in yeast, EMBO J. 17 (1998) 5374–5387, http://dx.doi.org/10.1093/emboj/17.18.5374.

[56] M. Knop, K. Siegers, G. Pereira, W. Zachariae, B. Winsor, K. Nasmyth, et al., Epitope tagging of yeast genes using a PCR-based strategy: more tags and improved practical routines, Yeast 15 (1999) 963–972, http://dx.doi.org/10.1002/(SICI)1097-0061(199907)15:10B<963::AID-YEA399>3.0.CO;2-W.

[57] S. Brenner, The genetics of *Caenorhabditis elegans*, Genetics 77 (1974) 71–94.

[58] R.S. Kamath, M. Martinez-Campos, P. Zipperlen, A.G. Fraser, J. Ahringer, Effectiveness of specific RNA-mediated interference through ingested double-stranded RNA in *Caenorhabditis elegans*, Genome Biol. 2 (2001)http://dx.doi.org/10.1186/gb-2000-2-1-research0002 (RESEARCH0002).

[59] V. Praitis, E. Casey, D. Collar, J. Austin, Creation of low-copy integrated transgenic lines in *Caenorhabditis elegans*, Genetics 157 (2001) 1217–1226.